Journal of Solid State Chemistry 182 (2009) 1717–1725

Contents lists available at ScienceDirect

Journal of Solid State Chemistry

journal homepage: www.elsevier.com/locate/jssc

Crystal structures and phase transitions of Sr_2CrSbO_6

A. Faik [a], J.M. Igartua [a,*], M. Gateshki [b], G.J. Cuello [a,c]

[a] Fisika Aplikatua II Saila, Zientzia Fakultatea, Euskal Herriko Unibertsitatea, P.O. Box 644, Bilbao 48080, Spain
[b] PANalytical, Lelyweg, Almelo 7600AA, Netherlands
[c] Ikerbasque and Institut Laue Langevin, BP 156, F-38042 Grenoble, France

ARTICLE INFO

Article history:
Received 10 January 2009
Received in revised form
30 March 2009
Accepted 5 April 2009
Available online 23 April 2009

Keywords:
Double perovskite
X-ray diffraction
Crystal structure
Phase transitions

ABSTRACT

Sr_2CrSbO_6 was synthesized by the conventional solid-state reaction process. X-ray powder diffraction (XRPD) and neutron powder diffraction (NPD) has been used to reinvestigate the structure at room temperature and to study the phase transitions at high- and low-temperature. Rietveld analysis revealed that Sr_2CrSbO_6 crystallizes at room temperature in a monoclinic system having a space group $I2/m$, with $a = 5.5574(1)$ Å; $b = 5.5782(1)$ Å; $c = 7.8506(2)$ Å and $\beta = 90.06(2)$, no $P2_1/n$ space group as was previously reported. The high-temperature study (300–870 K) has shown that the compound presents the following temperature induced phase-transition sequence: $I2/m$–$I4/m$–Fm-3m. The low-temperature study (100–300 K) demonstrated that the room-temperature $I2/m$ monoclinic symmetry seems to be stable down to 100 K.

1. Introduction

In recent years, the structural properties of double perovskite materials with general formula $A_2BB'O_6$ have been extensively studied [1–3]. The double perovskite structure can be represented as a three-dimensional network of alternating BO_6 and $B'O_6$ octahedra, with A-atoms occupying the 12-coordinated interstitial spaces between the octahedra. The aristotype structure of this family is cubic [4] with the space group Fm-3m (No. 225) [5]. However, due to a mismatch between the size of the A-site cation and the cuboctahedral space between the octahedra, many such materials undergo one [6], two [7] or even more [8] structural phase transitions at different temperatures. These structural transformations can be conveniently described as changes in the way the BO_6 and $B'O_6$ octahedra are rotated with respect to the crystallographic axes of the material to accommodate the size of the A-site cations [9,10]. In previous articles [11–13], we studied the structural phase transitions occurring in the materials with general formula Sr_2BWO_6 and B = Ni, Co, Zn, Ca, Mg or Cd. All of these tungsten oxide materials undergo temperature-induced phase transitions.

The family of strontium antimony oxides with double perovskite structure has attracted considerable attention because of the magnetic properties of some of its members, such as Sr_2FeSbO_6 [14,15]. From structural point of view, different symmetries have been reported for these materials: monoclinic, tetragonal, trigonal and cubic. Despite this variety, very few temperature-dependent structural studies have been conducted [16].

In [16] we have studied the structures of Sr_2AlSbO_6 and Sr_2CoSbO_6 with the X-ray powder diffraction (XRPD) method. At room temperature the crystal structure of Sr_2AlSbO_6 is cubic (Fm-3m). It was found that depending on the preparation conditions, the Al^{3+} and Sb^{5+} cations can be either entirely or partially ordered. In the case of the partially ordered Sr_2AlSbO_6 sample, the extension of cation ordering was estimated from the $hk\ell$-dependent broadening of the diffraction peaks and the results were interpreted as evidence of the formation of anti-phase domains in the material. Low-temperature Raman spectroscopic measurements demonstrated that the cubic phase of Sr_2AlSbO_6 is stable down to 79 K. The room-temperature crystal structure of Sr_2CoSbO_6 is trigonal (space group R-3, No. 148). At 470 K, however, the material undergoes a continuous phase transition and its structure is converted to cubic (space group Fm-3m). The studied Sr_2CoSbO_6 sample was partially ordered, but unlike Sr_2AlSbO_6, no indication of the formation of anti-phase domains was observed.

The aim of the present work is to analyze the structures and the possible structural phase transitions of Sr_2CrSbO_6, as there are no previous studies on the (high) temperature-dependent structural modifications of this material. This work is a part of a systematic study that we have undertaken on the $AA'BSbO_6$ (AA' = Ca_2, SrCa, Sr_2), and (B = Al, Sc, Cr, Fe, Co, La, Sm …) family of materials. Sr_2CrSbO_6 was first reported by Sleight and Ward [17], and subsequent X-ray diffraction (XRD) studies by Blasse [18]

* Corresponding author. Fax: +34946013500.
E-mail addresses: abdessamad.faik@ehu.es (A. Faik), josu.igartua@ehu.es (J.M. Igartua).

0022-4596/$ - see front matter © 2009 Elsevier Inc. All rights reserved.
doi:10.1016/j.jssc.2009.04.014

lead to the conclusion that this compound was cubic with 1:1 M-cation ordering. Woodward [19] reported Sr_2CrSbO_6 to be a monoclinic ordered double perovskite (space group $P2_1/n$, No. 14) based on the presence of small extra reflections and peak splitting in the XRPD diffractograms. Similar reflection splitting was observed in the XRPD data reported in [20], and they did full pattern Rietveld refinements (with constraints) using the $P2_1/n$ space group.

Finally, in [21], the most recent study on Sr_2CrSbO_6, the crystal structures at room-temperature and the magnetic properties of the double perovskites Sr_2CrSbO_6 and Ca_2CrSbO_6 were studied by X-ray and neutron powder diffraction (NPD) data. Rietveld refinements showed that the room-temperature crystal structure was monoclinic (space group $P2_1/n$), and that contained an almost completely ordered array of alternating CrO_6 and SbO_6 octahedra sharing corners, tilted along the three pseudocubic axes according to the Glazer notation $a-a-b+$. The monoclinic distortion was larger in Ca_2CrSbO_6 than in Sr_2CrSbO_6, which was associated with the tilting of the CrO_6 and SbO_6 octahedra, displaying tilting angles $\Theta = 13.5^\circ$ and $\Theta = 5.5^\circ$, respectively. Magnetization measurements and low-temperature NPD data showed that Sr_2CrSbO_6 is an antiferromagnet with a Néel temperature of 12 K, with an ordered magnetic moment of 1.64(4) μ_B per Cr^{3+}, being the propagation vector $k = 0$. This work is very important in relation to the magnetic properties of Ca_2CrSbO_6 as they report the first example of a ferromagnetic double perovskite containing a non-magnetic element in the B positions of the perovskite structure.

2. Experimental

2.1. Sample preparation

Sr_2CrSbO_6 was prepared by the standard method of solid-state reaction. Stoichiometric amounts of the reacting compounds were mixed according to the following chemical reaction: $2SrCO_3{+}1/2Cr_2O_3{+}1/2Sb_2O5 \rightarrow Sr_2CrSbO_6{+}2CO_2$.

The reacting compounds had the following purities: $SrCO_3$ (99.995%), Cr_2O_3 (99.99%) and Sb_2O_5 (99.99%). All compounds were used as received from Sigma-Aldrich. The starting materials were mixed and ground in an agate mortar with acetone and subsequently heated in air, in alumina crucibles. The following heat treatment was used: 6 h at 870 K, to eliminate the organic materials; 24 h at 1270 K; 24 h at 1470 K and 24 h at 1670 K; the final sintering was carried out at 1770 K for 72 h. After each heating, the samples were cooled down slowly (3 K/min); and reground (re-mixed) to improve homogeneity. In order to control the quality of the obtained material, X-ray diffraction measurements were performed after each heating. A small amount ($\approx$1.18% weight fraction) of the impurity $Sr_2Sb_2O_7$ was found in the final material: this impurity was included as a known additional phase in the Rietveld refinements of the structure of the studied compound.

2.2. Diffraction measurements and data analysis

High-quality room-temperature diffraction data were obtained on a Bruker D8 Advance diffractometer equipped with a primary germanium parafocusing monochromator and Bragg-Brentano geometry, using Cu$K\alpha1 = 1.5406$ (Å) radiation. A Sol-X energy dispersive detector was used, with a detection window optimized for Cu$K\alpha1$, in order to avoid the fluorescence radiation from the samples. The data were collected between 15° and 110° in 2θ, with steps of 0.01° (2θ) and a counting time of 12 s per step.

Low and high temperature diffraction data from Sr_2CrSbO_6 were collected on a similar diffractometer, but equipped with a Våntec high speed one-dimensional detector (with 3° of angular aperture), using Cu$K\alpha$ radiation. A TC-wide range temperature chamber of MRI with direct sample cooling and temperature stability of 0.5 K was used, between 110 and 300 K. An Anton Paar HTK2000 high-temperature chamber with direct sample heating (Pt filament) and a temperature stability of 0.5 K was used. The specimens for low and high temperature measurements were prepared by mixing the material under study with acetone. Then, the mixture was 'painted' over the sample holder block (low-temperature) or Pt-strip heater (high-temperature) of the evacuated chamber. To obtain reliable values for the unit cell parameters in the whole temperature-range from 110 to 870 K, 19 diffraction patterns from 110 to 300 K, with a temperature step of 15 K and 57 diffraction patterns, were collected between 310 and 870 K, with a temperature step of 10 K; all of them covering the 15°–120° 2θ interval. The diffraction peaks from the Pt sample heater that are present in the high temperature diffractograms were excluded from the refinements.

Neutron diffraction measurements were performed with the D20 high-intensity, medium-resolution instrument at Institut Laue–Langevin (Grenoble, France). The diffraction profiles were collected in the range $2\theta = 0°$–$160°$ with a neutron wavelength of 1.3 Å, between 300 and 750 K. The monochromator was Cu(200), with $\Delta d/d \approx 16 \times 10^{-3}$ resolution . This instrument is equipped with a detector that covers 153.4° in 2θ space and is made of 1534 ^{3}He cells [22]. The samples were placed in a vanadium capillary of 5 mm in diameter. Continuous heating with a rate of 1 °C/min was used. The coherent scattering lengths for Sr, Cr, W and O were 8.24, 3.635, 4.77 and 5.805 fm, respectively.

The Rietveld refinement of the structures was performed using the WinPlotr/FullProf package [23]. The peak shape was described by a pseudo-Voigt function, and the background level was modeled using a polynomial function. The refined parameters were: scale factor, zero shift, lattice constants, peak profile, asymmetry parameters, atomic positions and independent isotropic atomic displacement parameters. In the case of the neutron data the resolution function provided at the instrument was used.

3. Results and disscusion

3.1. Room-temperature structure

We have calculated the tolerance factor for Sr_2CrSbO_6, using ionic radii from [24]: $t = 1.000$. This value is between the values calculated for Sr_2CoSbO_6 [16], $t = 1.002$, and for Sr_2GaSbO_6 [25], $t = 0.999$. Being the three values so close, and knowing that the symmetries of Sr_2CoSbO_6 and Sr_2GaSbO_6 are R-3 and $I4/m$, respectively, we have tried both space groups as the starting models for the room-temperature refinements of the structure of Sr_2CrSbO_6.

In Table 1 we show four 2θ ranges and the corresponding ($hk\ell$) indices for the $I2/m$ (monoclinic, No. 12, non-standard setting of $C2/m$), $I4/m$, R-3 and Fm-3m (the aristotype cubic symmetry) space groups. In Fig. 1 we show sections, at two of those intervals, of the experimental (symbols), calculated (line) powder diffraction profiles for the Rietveld refinements of Sr_2CrSbO_6, at room temperature, using a structural model with the three different space groups: $I2/m$, $I4/m$ and R-3. In Fig. 1a and b we compare the monoclinic and the tetragonal space groups, and in Fig. 1c and d, the monoclinic and the trigonal. The important point in those comparisons is the splitting, which are evident, and from which neither the tetragonal nor the trigonal symmetries should

be assigned, despite the high tolerance factor found for the title compound.

It is known [10] that the diffraction pattern for a compound that has $P2_1/n$ symmetry must have reflections indicative of A-cation displacements (eeo), in-phase tilting distortions (ooe), out-of-phase tilting distortions and cation ordering (ooo). As revealed by the above careful examination of the peak splitting patterns from our XRPD diffractograms the unit cell is monoclinic, but the absence of reflections with (ooe) cubic indices indicates that there is no in-phase tilting. Besides, the usually small reflections corresponding to atomic displacements (eeo) are not observed; only (eee) and (ooo) reflections can be observed when the NPD pattern (Fig. 2b) is indexed with a doubled cubic lattice parameter. Thus, the peak splitting pattern and cubic Miller indices indicate that the true symmetry of the compound is $I2/m$, and not $P2_1/n$ as has been assigned very recently [21], or as it was pointed out in [19].

Another fact that corroborates the $I2/m$ space group assignment can be inferred by comparing the reflection conditions for the two monoclinic space groups. A compound with $I2/m$ symmetry must show ($hk\ell$) reflections with $h+k+\ell=2n$ Table 2 lists the first four reflections corresponding to in-phase tilting and cation displacements in the cubic unit cell and their corresponding monoclinic indices. Those peaks are not observed in the diffraction data (shown on XRPD and NPD data in Fig 2a and b, respectively), indicating that correct space group symmetry for Sr_2CrSbO_6 is $I2/m$.

Refinement results for the XRPD data with the $I2/m$ space group are given in Table 3. The mean interatomic distances and some selected bond angles are listed in Table 4. The $I2/m$ space group allows for 1:1 positional ordering of the B and B′ cations to form a rock-salt sub-lattice of corner-shared CrO_6 and SbO_6 octahedra. The Sr^{2+} cations are located in the cavities formed by the corner-sharing octahedra, and the average Sr–O distance

Table 1
2θ ranges and the ($hk\ell$) indices of the reflections for the $I2/m$, $I4/m$, R-3m and Fm-3m (the ideal cubic symmetry) space groups.

Peak (2θ, deg)	$I2/m$	$I4/m$	R-3	Fm-3m
39.2–40.2	022	022		222
	−202			
	202			
45.6–46.6	220		024	400
	004			
84.2–86.2	044	044		444
	−404			
	404			
101–105	440		048	800
	008			

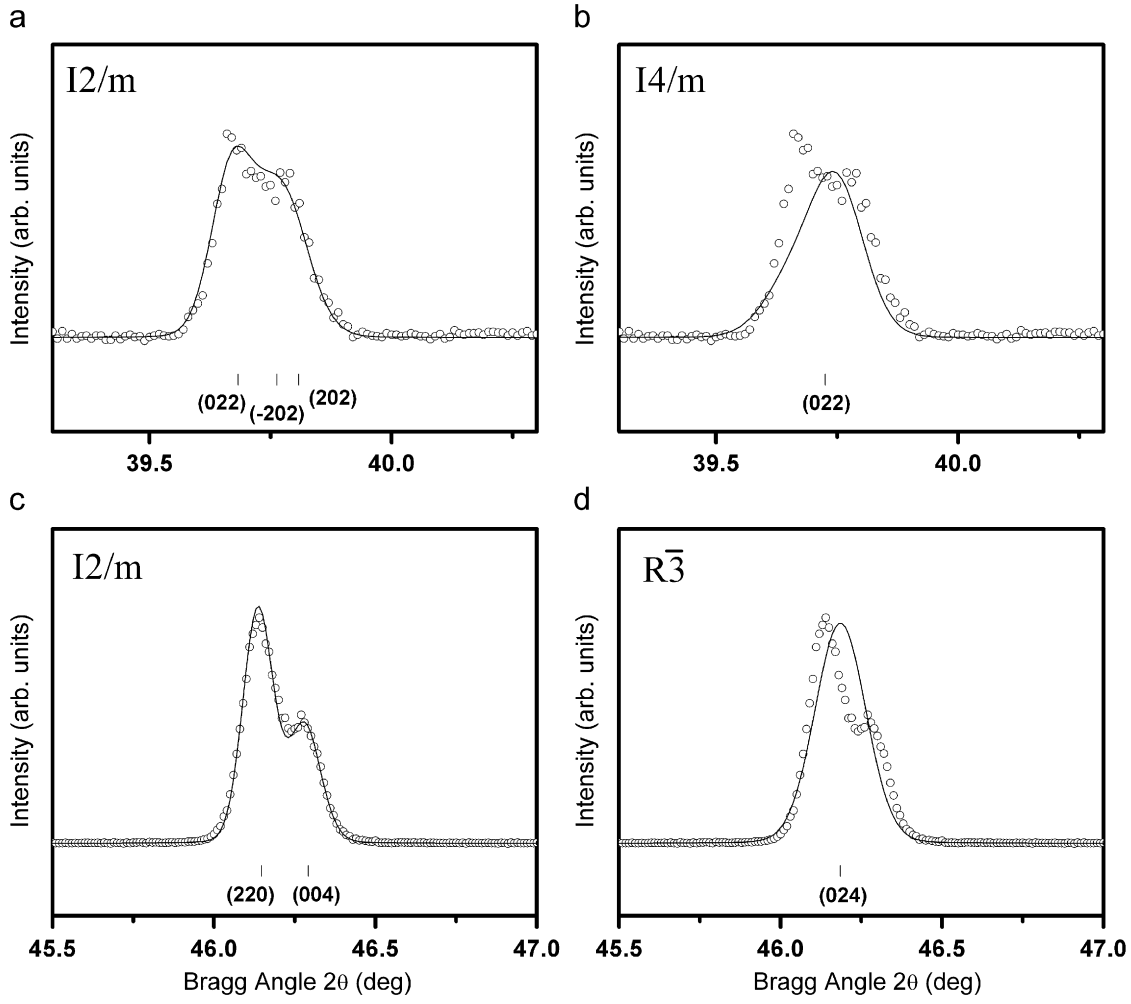

Fig. 1. (a) and (b) Sections of the diffractogram of the XRPD measurements refined in the $I2/m$ and $I4/m$ space groups, respectively, to show that the tetragonal symmetry does not take into account the observed splitting. (c) and (d) Another section of the diffractogram comparing the results of the refinements using the $I2/m$ and the R-3 space groups. The trigonal space group does not take into account the observed splitting.

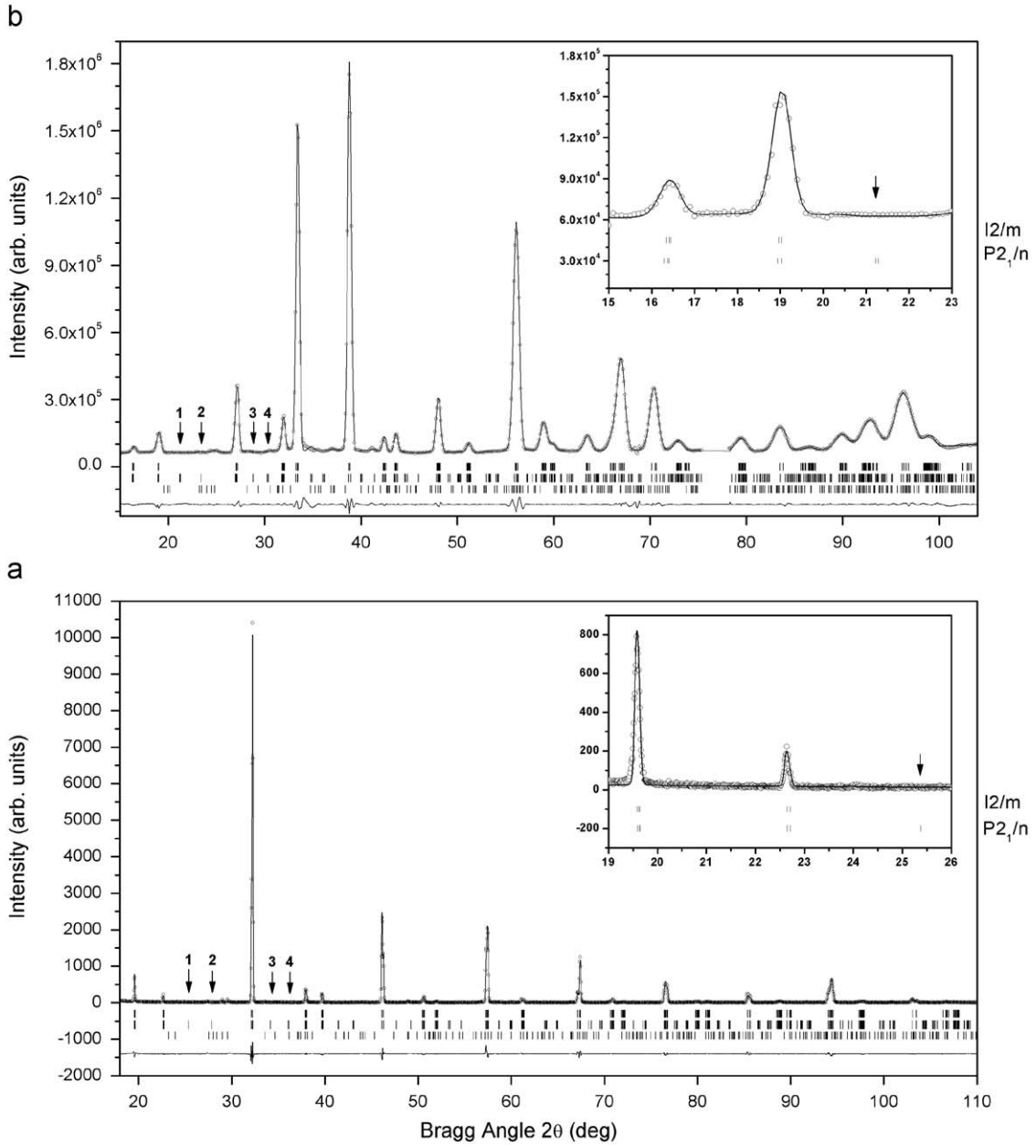

Fig. 2. (a) Experimental (symbols) (XRPD), calculated (line) and difference powder diffraction profiles for the Rietveld refinement of Sr_2CrSbO_6 at room temperature using a structural model with $I2/m$ space group. The impurity $Sr_2Sb_2O_7$ (1.18%) is included as a known additional phase. The vertical bars indicate the Bragg reflections: those in the top row correspond to the $I2/m$ space group; those in the middle row, to $P2_1/n$, and the ones in the bottom row, correspond to the impurity. Arrows indicate the positions of the reflections summarized in Table 2. Inset shows in detail the absence of the (double) peak of the form $h+k+\ell = 2n+1$, corresponding to the $P2_1/n$ symmetry. (b) Experimental (symbols), calculated (line) and difference neutron powder diffraction profiles for the Rietveld refinement of Sr_2CrSbO_6 at room temperature using a structural model with $I2/m$ space group. The same comments apply.

Table 2
List of the first four reflections corresponding to A-cation displacements (eeo) and to in-phase tilting distortions (ooe) in the cubic unit cell and their corresponding monoclinic indices.

Peak	$\approx 2\theta$		Monoclinic indices ($P2_1/n$)	Cubic $h\,k\,\ell$	
	XRPD	NPD		(eeo) A-cation displacement	(ooe) In-phase tilting
1	25	21.4	(−111) (111)	(−210)	
2	27	23.6	(012)		(−211)
3	34	29	(021)	(300), (221)	
4	36	30.5	(120) (210)	(−310)	

XRPD and NPD wavelengths are 1.5406 and 1.3 Å, respectively.

Table 3
Crystal structure at room temperature (XRPD).

Atom	x	y	z	B(Å^2)	Occupancy
Sr	0.4999(1)	0	0.2504(3)	0.71(3)	1.00
Sb1/Cr2	0	0	1/2	0.24(3)	0.994(1)/0.006(1)
Cr1/Sb2	0	0	00.53(6)	0.53(6)	0.994(1)/0.006(1)
O1	−0.039(4)	0	0.249(5)	1.10(3)	1.00
O2	0.246(2)	0.249(4)	0.015(5)	1.10(3)	1.00

The atomic positions were refined in the *I*2/*m* space group. The cell parameters are: $a = 5.5574(1)$ Å; $b = 5.5782(1)$ Å; $c = 7.8506(2)$ Å; $\beta = 90.06(2)$; $V = 243.37(1)$ Å^3 for the XRPD. Reliability factors (XRPD): $R_p =$ 10.0%, $R_{wp} =$ 17.5%, $R_{exp} =$ 14.1%, χ^2: 1.54, $R_{Bragg} = 2.63$.

Table 4
Main bond distances (Å) and selected angles (deg) for Sr_2CrSbO_6 from XRPD at room temperature.

	Sr_2CrSbO_6
SrO_{12} polyhedra	
Sr–O1	2.955(1)
Sr–O1	2.602(5)
Sr–O1 (× 2)	2.795(6)
Sr–O2 (× 2)	2.702(9)
Sr–O2 (× 2)	2.886(5)
Sr–O2 (× 2)	2.857(7)
Sr–O2 (× 2)	2.877(9)
Average distance	2.783(2)
Predicted distance	2.781
CrO_6 octahedra	
Cr–O1 (× 2)	1.959(8)
Cr–O2 (× 4)	1.948(7)
Average distance	1.952(4)
Predicted distance	1.9805
SbO_6 octahedra	
Sb–O1 (× 2)	1.982(5)
Sb–O2 (× 2)	1.996(4)
Average distance	1.991(8)
Predicted distance	2.0095
Sb–O1–Cr (× 2)	169(1)
Sb–O2–Cr (× 4)	173(1)
〈Cr–O–Sb〉	172

$rCr^{3+}(VI) = 0.615$ Å, $rSb^{5+}(VI) =$ 0.6 Å.

2.783 Å is typical for Sr^{2+} cations in a 12-coordinate environment. For the Sb–O bonds, the average value of the bond distances within the octahedra 1.991 Å are in good agreement with the value predicted by bond valence calculations 2.0095 Å; and for the Cr–O bonds, the average value 1.952 Å is somewhat shorter than the expected one 1.9805 Å. The small discrepancies (bigger in the case of the Cr octahedra) can be associated to the grade of disorder in the B-site present in the material.

In previous works published on double perovskite oxides, it has been shown that the *I*4/*m* space group is not the "standard" room-temperature structure space group [26–28]. The monoclinic splitting is to be taken into account, but the space groups $P2_1/n$ and *I*2/*m* (another possible monoclinic space group, $a^0a^-a^-$ tilt system) give rise to the same splitting, although the former gives also rise to primitive-cell reflections: $(hk\ell)$ with $h + k + \ell = 2n + 1$. These kind of primitive reflections usually are very weak, and from their presence undoubtedly a primitive lattice has to be assigned. Nonetheless, if they can't be seen in the diffractogram, as it is our case, a non-primitive cell can be assumed. In that assumption, if the *R*-factors do not increase in a nonphysical way, the higher symmetry is usually assigned.

We have checked the possible symmetry miss-assignment of the structure reported in [21], analyzing the possible presence of pseudosymmetry, making use of PSEUDO [29]. The results show that displacing the Sr cation by 0.003 Å and O1 by 0.111 Å (absolute units), the *I*2/*m* space group can be achieved (*I*2/*m* is a super group of index 2 of $P2_1/n$). As it has been shown [30,31] an overall displacement of 0.75 Å is taken as a good value to assure a mis-assignment of symmetry. Hence, changing slightly the location of the oxygens [21] and assigning the antimony cation a more realistic (lower) B_{iso} value, gives rise to the *I*2/*m* space group. Thus, our data show that the space group *I*2/*m* gives a better description of the room-temperature structure of Sr_2CrSbO_6 (at least for the sample we have worked with) than that reported with the $P2_1/n$ space group structure in [21]; moreover, with the former description no physical or chemical inconsistencies are remaining.

In Fig. 3 we show the projections along the cubic (simple) perovskite axes, ($[100]_p$, $[010]_p$ and $[001]_p$), corresponding to a section of the unit cell of the double perovskite with $A_2MM'O_6$ general formula in the *I*2/*m* and $P2_1/n$ space groups. The difference between both structural models consists in the losing of the tilt angle around the $[001]_p$ axis, which coincides with the *c* axis of the double perovskite.

3.2. Temperature-induced phase transitions: low- and high-temperatures

Although Sr_2CrSbO_6 has been studied at low temperature [21], no structural phase transition has been reported and, as far as we know, this is the first time that the temperature-induced structural phase-transitions at high temperature are reported in this compound. We have explored the low-temperature interval, 110–300 K, and from our XRPD results we have to conclude that the room-temperature *I*2/*m* monoclinic symmetry seems to be stable down to at least 100 K.

In Fig. 4 we show the evolution of the scattering intensity with temperature for three 2θ intervals corresponding to (a) (444), (b) (800) and (c) (660) cubic (*Fm*-3*m*, space group) reflections. As it can be concluded from the figure, Sr_2CrSbO_6 undergoes two successive temperature-induced phase transitions taking place at 500 and 660 K, respectively. The first one, discontinuous, changes the symmetry from monoclinic *I*2/*m* to tetragonal *I*4/*m*. The discontinuous character of the phase transition can be readily appreciated in Fig. 4b; nevertheless, in Fig. 4a we have represented the reflection that gives the difference between both space groups: (044), (–404), (404) in the *I*2/*m* space group go to a single reflection in I4/*m*, (044). The reflections shown in Fig. 4b are (440) and (008) in both space groups, *I*2/*m* and *I*4/*m*, but as they are interchanged in position, the transition is obvious. In Fig. 4c the continuous (see below) character of the *I*4/*m* to *Fm*-3*m* phase transition is "easily" appreciated: at that symmetry change, nearly all reflections increase intensity as all the splitting disappears.

In Fig. 5 we show the same 2θ intervals as in Fig. 4, but this time only the profile at a single temperature is plotted: (a) 110 K, (b) 310 K (both in the *I*2/*m* monoclinic phase), (c) 510 K (*I*4/*m* tetragonal phase) and (d) 670 K (*Fm*-3*m* cubic phase). The tetragonal splitting of the (800) cubic reflection (102°–104.5° interval (c) panel) is very clear; the interchange in the positions of the (008) and (440) *I*4/*m* tetragonal reflections going to (440) and (008) *I*2/*m* monoclinic is also true (same interval and (b) panel). From the comparison of the (a) and (b) panels the decreasing of the monoclinic splitting as temperature increases can be observed.

Finally, in Fig. 6 we plot the evolution with temperature of the cell parameters of Sr_2CrSbO_6 in the whole temperature range, from 110 to 870 K, as obtained from the refinements of

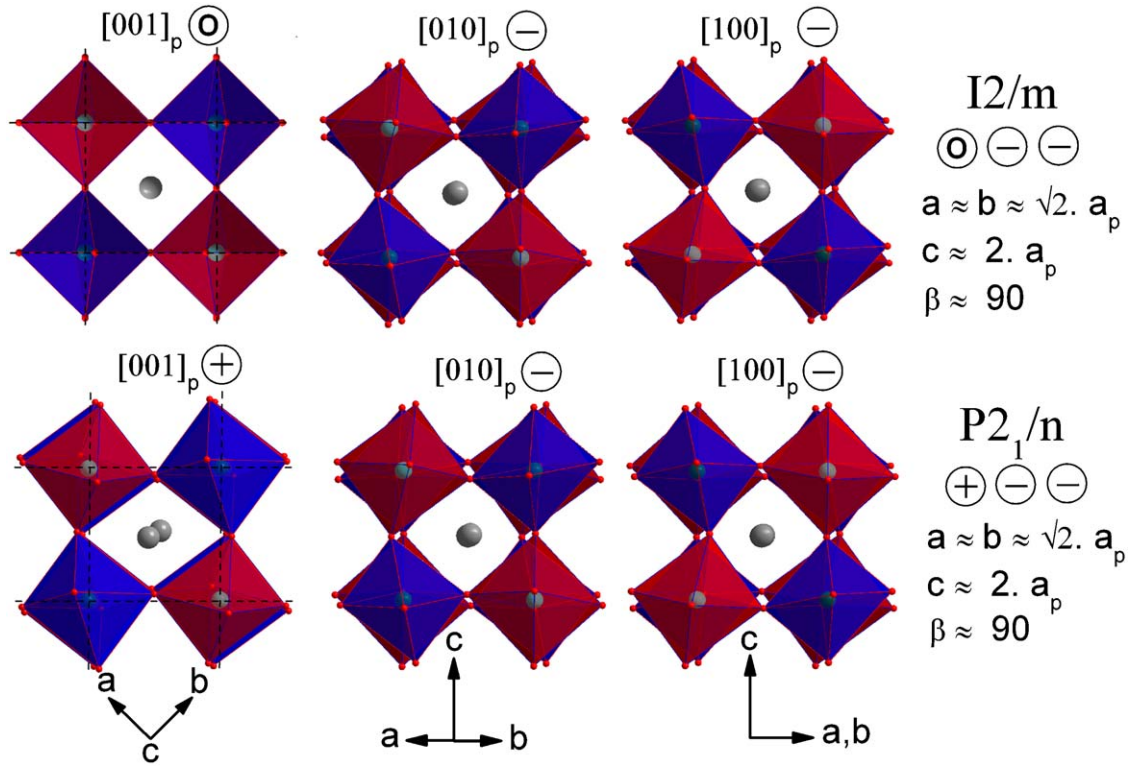

Fig. 3. Projections along the cubic (simple) perovskite axes, ($[100]_p$, $[010]_p$ and $[001]_p$), of a section of the unit cell of the double perovskite with $A_2MM'O_6$ general formula in the $I2/m$ and $P2_1/n$ space groups.

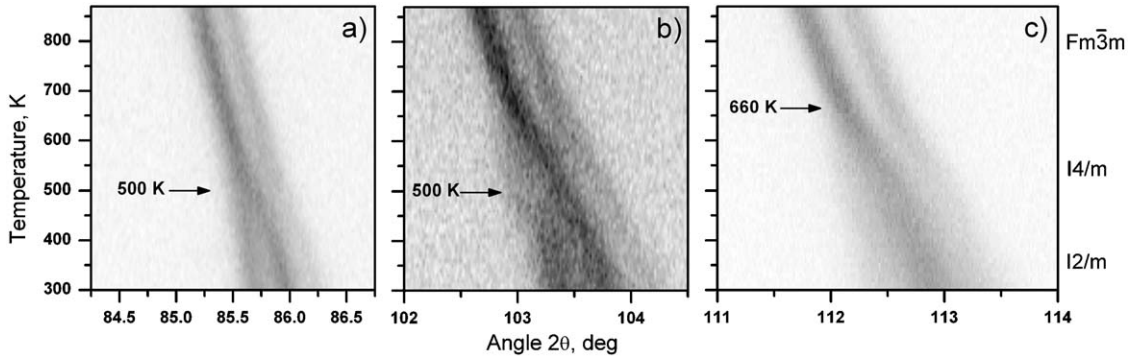

Fig. 4. Thermal evolution of the (a) (444), (b) (800) and (c) (660) cubic reflections as obtained from XRPD experiments. The scattered intensity is represented with shades of gray—black corresponds to high intensity, and white, to low intensity. In (a), the $I2/m$ monoclinic triplet [(044), (−404), (404)] converts to a single $I4/m$ tetragonal reflection: (044). In (b), two monoclinic reflections maintain as two tetragonal but with the positions interchanged, and, eventually, the tetragonal splitting disappears and the double reflection evolves to a single cubic one. (c) Temperature evolution of the (660) cubic reflections: the tetragonal splitting existing in the temperature range from 500 to about 660 K can be observed.

the XRPD data of three different measurements: the first one, a low temperature measurement from 110 to 300 K, represented in the figure by open squares; the second one, a high-temperature measurement from 300 to 870 K, represented in the figure by open circles; and the third one, a measurement using the low-temperature camera from the lowest to the highest temperatures, 110 and 700 K, at four temperatures as indicated, represented in the figure by stars. The evolution with temperature of the cell parameters is very similar to that observed for the members of the Sr_2MWO_6 family which show a two successive phase-transitions. Although in the tungsten containing family the low temperature monoclinic phase has the $P2_1/n$ space group and not $I2/m$, both space groups give rise to the nearly the same structural model (see Fig. 3): the extra $P2_1/n$ distortion is not appreciated in the cell parameters. The same is true for the cell parameters' evolution in the tetragonal phase: the characteristic feature of the tungsten family members is the negative thermal expansion of the c parameter, as is the case in the title compound.

Despite the fact that the XRPD and NPD measurements have been carried out obviously in different equipments, under different measuring conditions and using distinct ancillary equipment, they are in complete agreement. Although there is an obvious splitting in the monoclinic phase, the overlapping of the reflections in the NPD data makes impossible the structural determination: there is no enough resolution. The third set of XRPD measurements have been carried out to be able to extract structural data: shown in Table 5.

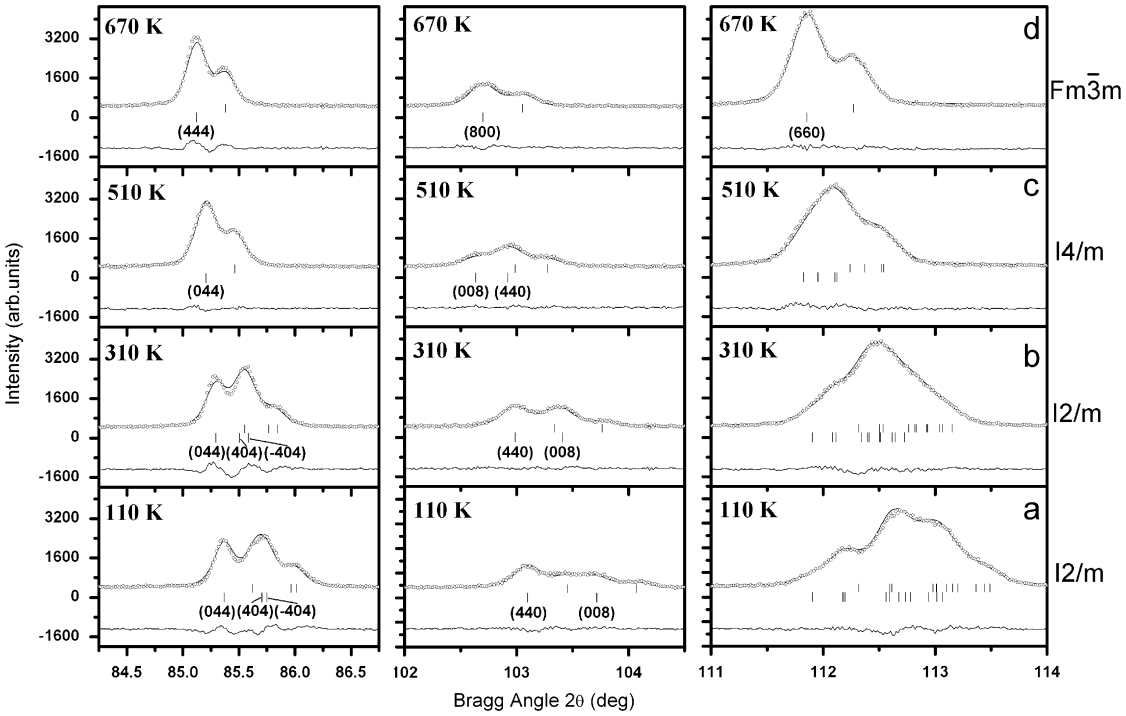

Fig. 5. The thermal evolution of the (444), (800) and (600) cubic reflections as determined from XRPD measurements are shown in left, middle and right column panels, respectively. Each panel represents a single profile section at a fixed temperature: (a) 110 K, (b) 310 K, (c) 510 K and (d) 670 K.

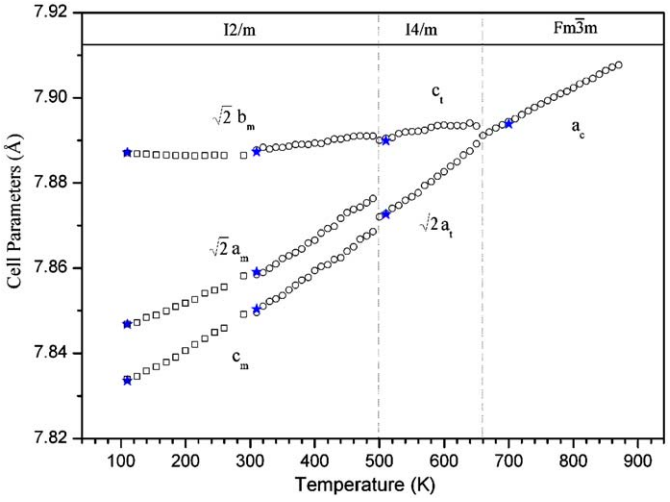

Fig. 6. The temperature evolution of the cell parameters of Sr_2CrSbO_6 as obtained from the three different XRPD measurement series: open circles up to 300 K, were obtained in the first low-temperature measurement; open circles from 300 to 900 K were obtained with the high-temperature camera, in both cases in the same conditions; finally, stars were obtained using the low-temperature camera and with a counting time in each step (long enough) so that we had the required statistics to determine the structure. The high-temperature structure of the compound is cubic (*Fm*-3*m*); below 660 K it transforms to tetragonal (*I*4/*m*); and at 500 K the compound transforms to monoclinic (*I*2/*m*).

Table 5
Crystal structure data and refinement results for Sr_2CrSbO_6 from XRPD at 110, 310, 510 and 700 K.

Temperature (K)		110	310	510	700
Space group		*I*2/*m*	*I*2/*m*	*I*4/*m*	*Fm*-3*m*
Sb1/Cr2		0, 0, 1/2	0, 0, 1/2	0, 0, 1/2	0, 0, 0
Cr1/Sb2		0, 0, 0	0, 0, 0	0, 0, 0	0, 0, 1/2
Sr	*x*	0.5008(1)	0.4978(2)	0	1/4
	y	0	0	1/2	1/4
	z	0.2493(2)	0.2493(3)	1/4	1/4
O_1	*x*	−0.0627(6)	−0.0638(8)	0	0.2584(3)
	y	0	0	0	0
	z	0.2473(8)	0.2468(2)	0.2431(3)	0
O_2	*x*	0.2484(8)	0.2469(8)	0.2825(2)	–
	y	0.2362(9)	0.2379(7)	0.2053(9)	–
	z	0.0279(8)	0.0256(8)	0	–
B (Å^2)	Sb1, Cr2	0.28(2)	0.44(2)	0.68(2)	0.58(2)
	Cr1, Sb2	0.75(4)	0.92(4)	1.11(3)	1.22(4)
	Sr	0.52(2)	0.81(2)	1.16(2)	1.40(2)
	O1, O2	0.34(7)	0.73(8)	1.61(8)	2.15(1)
Cell parameters					
a (Å)		5.5485(1)	5.5572(1)	5.5668(1)	7.8939(1)
b (Å)		5.5770(1)	5.5772(1)	–	–
c (Å)		7.8336(1)	7.8503(1)	7.8899(1)	–
β (deg)		89.97(4)	90.04(3)	–	–
V (Å^3)		242.40(1)	243.31(1)	244.50(1)	491.89(1)
Reliability factors					
R_p (%)		7.80	4.29	4.39	5.95
R_{wp} (%)		8.87	6.08	6.08	8.26
R_{Bragg} (%)		4.19	2.90	2.97	2.95
χ^2 (%)		4.48	4.40	4.18	7.83

We have analyzed the temperature evolution of the tetragonal structure, as deduced from the NPD data, until it undergoes the phase transition to the cubic phase, using the AMPLIMODES program [32]. AMPLIMODES carries out a symmetry-mode analysis of a displacive phase transition. Starting from the experimental structures of the high- and low-symmetry phases, the program determines the global structural distortion that relates the two phases. The symmetry modes compatible with the symmetry break are then calculated. Their orthogonality allows the decomposition of the global distortion, obtaining the amplitude of each symmetry mode, as well as the corresponding eigenvectors. In the tetragonal (*I*4/*m*) to cubic (*Fm*-3*m*) phase transition there are three

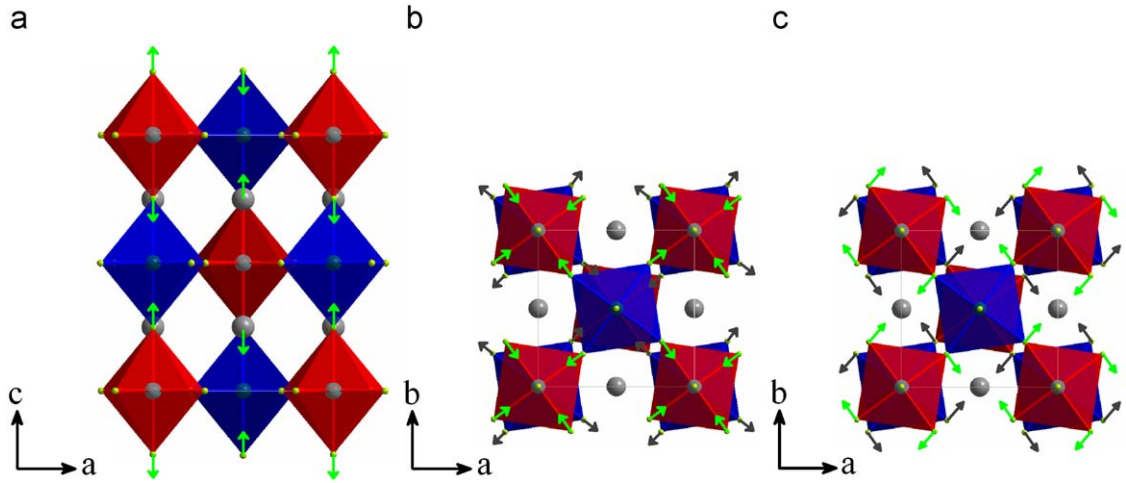

Fig. 7. (a) and (b) The components of the GM^{3+} mode, responsible for the breaking of the symmetry to the *I*4/*mmm* tetragonal space group from the *Fm*-3*m*, observed experimentally at high. This mode involves the movements of all the oxygen atoms in the octahedra: those located in the (00*z*) positions move to the center (or out of) of the octahedra, as shown in (a); and the oxygen atoms located in the *xy* plane move outwards (inwards) along the diagonals of the basal plane of the octahedra (b). As the octahedra are corner sharing if one octahedra stretches the other one expands. (c) On the other hand, the mode GM^{4+} is responsible for the breaking of the symmetry down to the *I*4/*m* space group, and involves movements only of the oxygen atoms located in the *xy* plane (c): those displacements can be viewed as rotations (tilts) of the octahedra around the tetragonal axis.

unidimensional modes: GM^{1+}, GM^{3+} and GM^{4+}. The GM^{3+} mode is responsible for the breaking of the symmetry to the *I*4/*mmm* tetragonal space group (intermediate between the *Fm*-3*m* and the *I*4/*m*, observed experimentally at high and low temperature, respectively). This mode involves the movements of all the oxygen atoms in the octahedra, in a way that those located in the (00*z*) positions move to the center of the octahedra; and the oxygen atoms located in the *xy* plane move outwards along the diagonals of the basal plane of the octahedra (see Fig. 7a and b). On the other hand, the mode GM^{4+} is responsible for the breaking of the symmetry down to the *I*4/*m* space group, and involves movements only of the oxygen atoms located in the *xy* plane (Fig. 7c). We show the amplitude of each mode in Fig. 8a. It can be readily appreciated that the amplitude of the first ones, the totally symmetric one (GM^{1+}) and GM^{3+} are negligible, of the order of magnitude of the error in the data, and that they maintain at a constant value. On the other hand, the GM^{4+} mode amplitude is considerable and shows a clear evolution with temperature: diminishes as temperature increases, and at the transition temperature (650 K) it reaches its lowest (non-null) value.

This is the typical behavior of the primary order parameter of a continuous phase transition [33]: continuous decreasing and a smooth change to zero at the critical temperature. Indeed, in the same figure, in the right axis, we have plotted the evolution of the angle of rotation of the octahedra around the tetragonal axis (the only distortion allowed by symmetry in the *I*4/*m* tetragonal phase, $a^0a^0c^-$ tilt system): the matching of both magnitudes is perfect, indicating that they are proportional and, thus, showing that the rotation of the octahedra around the tetragonal axis is the primary order parameter associated to the tetragonal-to-cubic phase transition.

All these facts allow us concluding that the symmetry changes taking place in Sr_2CrSbO_6, which belongs to the $Sr_2M^{3+}Sb^{5+}O_6$ system, have the same origins that those driving the structural change (tetragonal-to-cubic) in the $Sr_2M^{2+}W^{6+}O_6$ family [13]; that is, the tetragonal distortion of the unit cell is the result of an homogeneous strain coupled to the order parameter (the angle of rotation of the octahedra around the tetragonal axis). The transition takes place due to the mismatch of the Sr^{2+} cation and the cubo-octahedral interstitial space between the MO_6 and SbO_6 octahedra, and, also, due to the softening of the T^{4+} phonon [34].

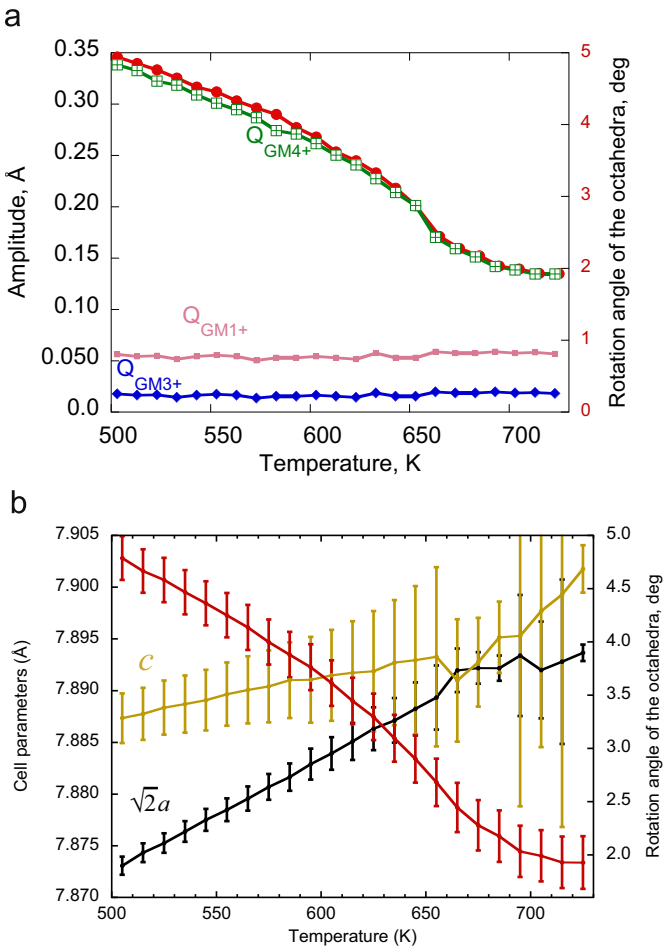

Fig. 8. (a) The temperature evolution of the amplitudes of the GM^{1+}, GM^{3+} and GM^{4+} modes, in the left axis, as calculated by AMPLIMODES from the NPD data, and in the right axis, temperature evolution of the angle of rotation of the octahedra around the tetragonal axis. Both magnitudes are proportional, and show the typical behavior of a primary order parameter. The temperature at which the tetragonal structure disappears is 625 K (there is a temperature-shift in comparison to the XRPD data). (b) The temperature evolution of the cell parameters $a\sqrt{2}$ and *c*, in the left axis; in the right one, the evolution with temperature of the rotation angle of the octahedra around the tetragonal axis, as in (a).

4. Conclusions

The double perovskite oxide Sr_2CrSbO_6 was prepared and the structure at room temperature was found to be monoclinic with space group $I2/m$, which is different from the previously suggested $P2_1/n$, and maintains its symmetry on cooling down to 100 K. The evolution with temperature of the structure of this material at high temperature shows the presence of two phase transitions: a discontinuous one from $I2/m$ to $I4/m$, at 500 K and a continuous one from $I4/m$ to $Fm\text{-}3m$, at 660 K.

Acknowledgments

This work was done in part under project numbers: UPV 0063.310-13564/2001-2007 and MAT2008-05839/MAT. The authors thank ILL for the beamtime allocation and the staff of D20 for their kind help and technical assistance.

References

[1] K.-I. Kobayashi, T. Kimura, H. Sawada, K. Terakura, Y. Tokura, Nature 395 (1998) 677–680.
[2] M. DeMarco, H.A. Blackstead, J.D. Dow, M.K. Wu, D.Y. Chen, E.Z. Chien, H. Haka, S. Toorongian, J. Fridmann, Phys. Rev. B 62 (2000) 14301–14303.
[3] Y. Todate, J. Phys. Chem. Solids B 60 (1999) 1173.
[4] P.M. Woodward, Acta Cryst. B 53 (1997) 32.
[5] International Tables for Crystallography, vol. A, T. Hahn (Ed.), Kluwer, Dordrecht, 2002.
[6] O. Chmaissem, R. Kruk, B. Dabrowski, D.E. Brown, X. Xiong, S. Kolesnik, J.D. Jorgensen, C.W. Kimball, Phys. Rev. 62 (2000) 14197.
[7] K. Yamamura, M. Wakeshima, Y. Hinatsu, J. Solid State Chem. 179 (2006) 605–612.
[8] L.O. San Martín, J.P. Chapman, E. Hernández-Bocanegra, M. Insausti, M.I. Arriortua, T. Rojo, J. Phys.: Condens. Matter 16 (2004) 3879–3888.
[9] A.M. Glazer, Acta Cryst. B 28 (1972) 3384;
A.M. Glazer, Acta Cryst. A 31 (1975) 756–762.
[10] C.J. Howard, B.J. Kennedy, P.M. Woodward, Acta Cryst. B 59 (2003) 463–471.
[11] M. Gateshki, J.M. Igartua, E. Hernández-Bocanegra, J. Phys.: Condens. Matter 15 (2003) 6199–6217.
[12] M. Gateshki, J.M. Igartua, J. Phys.: Condens. Matter 16 (2004) 6639–6649.
[13] M. Gateshki, J.M. Igartua, A. Faik, J. Solid State Chem. 180 (2007) 2248–2255.
[14] E.J. Cussen, J.F. Vente, P.D. Battle, T.C. Gibb, J. Mater. Chem. 7 (1997) 459–463.
[15] N. Kashima, K. Inoue, T. Wada, Y. Yamaguchi, Appl. Phys. A 74 (2002) S805–S807.
[16] A. Faik, M. Gateshki, J.M. Igartua, J.L. Pizarro, A. Grzechnik, M. Insausti, R. Kaindl, J. Solid State Chem. V 181 (2008) 1759–1766.
[17] A. Sleight, R. Ward, Inorg. Chem. 3 (1964) 292.
[18] G. Blasse, J. Inorg. Nucl. Chem. 27 (1965) 993–1003.
[19] P.W. Woodward, Ph.D. Dissertation, Oregon State University, Corvallis, OR, 1997.
[20] P.W. Barnes, Ph.D. Dissertation, Ohio State University, Corvallis, OR, 2003.
[21] M. Retuerto, M. García-Hernández, M.J. Martínez-Lope, M.T. Fernández-Díaz, J.P. Attfield, J.A. Alonso, J. Mater. Chem. 17 (2007) 3555–3561.
[22] T.C. Hansen, P.F. Henry, H.E. Fischer, J. Torregrossa, P. Convert, Meas. Sci. Technol. 19 (2008) 034001.
[23] J. Rodríguez-Carvajal, Physica B 192 (1993) 55–69.
[24] R.D. Shannon, Acta Cryst. A 32 (1976) 751.
[25] M.W. Lufaso, R.B. Macquart, Y. Lee, T. Vogt, H.C. Loye, J. Phys.: Condens. Matter 18 (2006) 8761–8780.
[26] G.Y. Liu, G.H. Rao, X.M. Feng, H.F. Yang, Z.W. Ouyang, W.F. Liu, J.K. Liang, J. Alloys Compd. V 353 (2003) 42–47.
[27] R.S. Liu, T.S. Chan, S.F. Hu, J.G. Lin, C.Y. Huang, J. Magn. Magn. Mater. 239 (2002) 164–166.
[28] A. Pena, J. Gutiérrez, L.M. Rodríguez-Martínez, J.M. Barandiarán, T. Hernández, T. Rojo, J. Magn. Magn. Mater. 254–255 (2003) 586–588.
[29] E. Kroumova, M.I. Aroyo, J.M. Pérez-Mato, S. Ivantchev, J.M. Igartua, H. Wondratschek, J. Appl. Cryst. 34 (2001) 783–784.
[30] J.M. Igartua, M.I. Aroyo, J.M. Pérez-Mato, Phys. Rev. B 54 (1996) 12744–12752.
[31] E. Kroumova, M.I. Aroyo, J.M. Pérez-Mato, R. Hundt, Acta Cryst. B 57 (2001) 599–601.
[32] M.I. Aroyo, J.M. Pérez-Mato, C. Capillas, E. Kroumova, S. Ivantchev, G. Madariaga, A. Kirov, H. Wondratschek, Z. Kristallogr. 221 (1) (2006) 15–27.
[33] M. Gateshki, J.M. Igartua, J. Phys.: Condens. Mater. 15 (2003) 6749–6757.
[34] A. Tressaud, S. Khaïroun, J.P. Chaminade, M. Couzi, Phys. Status Solid 98 (1986) 417.